Journal of Materials Chemistry A

Accepted Manuscript

ROYAL SOCIETY OF CHEMISTRY

www.rsc.org/materialsA

Journal Name

ARTICLE TYPE

Cite this: DOI: 10.1039/xxxxxxxxxx

Photonic flash-annealing of lead halide perovskite solar cells in 1 ms†

Joel Troughton,[a] Matthew J. Carnie,[a] Matthew L. Davies,[a] Cécile Charbonneau,[a] Eifion H. Jewell,[a] David A. Worsley[a] and Trystan M. Watson*[a]

Received Date
Accepted Date

DOI: 10.1039/xxxxxxxxxx

www.rsc.org/journalname

An extremely fast annealing technique for mixed-halide perovskite solar cells is presented. Using photonic flash sintering, we have demonstrated that a spin-coated perovskite precursor may be fully annealed in as little as 1 ms. Devices annealed in 1.15 ms yielded power conversion efficiencies (PCEs) of upto 11.3% compared to 15.2% for samples annealed for 90 minutes on a hotplate.

1 Introduction

Since their inception in 2009,[1] followed by breakthrough developments in 2012;[2?] solar cells based on organic-inorganic metal halide perovskite have experienced a meteoric rise in interest within the photovoltaic community and beyond. Power conversion efficiencies (PCEs) for perovskite solar cells (PSCs) have risen from 9.7%[2] to certified 20.1%, a rate that has eclipsed other photovoltaic technologies. The deposition and heat treatment of the perovskite layer is a key step in producing efficient devices and several processing methods exist which yield perovskite films with varying properties: one-step coating of both inorganic and organic precursors,[2?–5] sequential deposition of precursors,[6–8] vacuum evaporation of precursors,[9] vapor-assisted deposition of precursors[10] and solvent-assisted crystallisation.[11] A common step required for the majority of these deposition processes is a thermal anneal of the perovskite layer in order to drive off any residual solvent from the precursor and/or to change the morphology of the perovskite microstructure to a more favourable configuration.[12] Depending on the perovskite preparation technique used, the annealing process may take between 5 and 120 minutes.[2,3,12?–16] This time frame required to anneal the perovskite layer may pose a potential bottleneck in the eventual commercial production, aspirational high volume and continuous manufacture of such devices. We have previously demonstrated that comparable PCEs to devices annealed in 45 minutes in a conventional oven could be achieved in as little as 2.85 s by using an intense burst of near-infrared (NIR) radiation from commercially available tungsten-halogen lamps.[17] NIR emitters have a peak output at around 1,000 nm whereas "photonic" curing boasts broadband spectral output between 200 and 1,000 nm and is employed in this study to anneal efficient perovskite films in as little as 1 ms. This curing method has been demonstrated to be effective at rapidly sintering nanoparticle inks,[18–20] metal oxide scaffolds,[21] as well as improving performance when used to selenise $CuInSe_2$ films in copper indium gallium selenide (CIGS) solar cells.[22] In this system, a xenon strobe lamp, with a spectral output close to that of a blackbody, can be adjusted by varying the voltage across the bulb, as well as changing the duration of the flash pulse in order to carefully control the amount of energy irradiated, optimising these processes minimises the total energy and time needed to complete annealing. We demonstrate that mesoporous Al_2O_3-infiltrated $CH_3NH_3PbI_{3-x}Cl_x$ perovskite films can be fully annealed in atmospheric conditions in as little as 1 ms. In this study we achieved a maximum of 11.3% PCE device annealed in 1.15 ms compared to 15.2% PCE for an otherwise identical cell annealed for 90 min on a hotplate under a nitrogen atmosphere. These "ultra-fast" annealing times were obtained using a commercially available photonic curing system designed to thermally reduce metallic inks for printed electronics applications. We explore the implications of altering the annealing process window in order to obtain highly crystalline films and compare these to typical devices annealed on a hotplate. In addition, we characterise photonic annealed perovskite films using x-ray diffraction spectroscopy (XRD) and local photoluminescence spectroscopy (PL) to determine the impact of fast annealing on film formation, morphology and crystal growth. Transient Photovoltage (TPV) and Transient Photocurrent (TPC) decays were also measured to gain information on how the differing film morphologies and thicknesses obtained from conventional and photonically annealed perovskite films affects recombination in these devices.

[a] SPECIFIC - Swansea University College of Engineering, Bay Campus, Swansea SA1 8EN, United Kingdom. E-mail: T.M.Watson@swansea.ac.uk

† Electronic Supplementary Information (ESI) available: [details of any supplementary information available should be included here]. See DOI: 10.1039/b000000x/

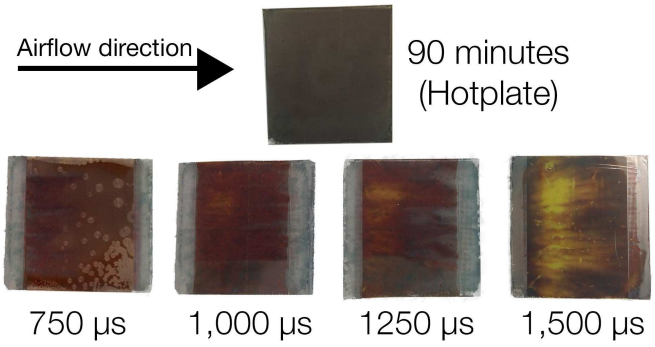

Fig. 1 Composed photograph of photonic annealed perovskite samples (28 mm × 28 mm) with increasing flash durations at 500 V lamp voltage, as well as a film annealed conventionally using a hotplate.

2 Results & Discussion

Initial visual observations were made of photonically annealed perovskite films in order to determine flash times with an ideal film being assumed to have a uniform, dark brown appearance similar to that of conventionally annealed films. Figure 1 shows 4 such films processed with increasing flash durations at a fixed lamp voltage as well as a sample annealed for 90 minutes on a hotplate at 100 °C under nitrogen. It is interesting to note the difference in transparency along opposite edges in the photonic annealed samples: these regions are masked from the light source by metal strips used to secure the glass sample to the instrument platform, consequently, these covered areas do not crystallise to form the perovskite structure. This effect demonstrates that annealing is driven only by direct exposure of the precursor film to a photonic pulse, thus excluding the possibility of indirect heating of the precursor via the substrate.

Similar to other rapid annealing techniques,[17] Figure 1 demonstrates how careful tuning of the annealing time is required for optimal device appearance. The 750 μs annealed film shows spherulitic formations arising from un-annealed precursor solution reacting with moisture within the air, demonstrating that the film has not been fully annealed into the desired $CH_3NH_3PbI_3$ perovskite material. Conversely, the 1,500 μs annealed film exhibits yellow discolouration which is indicative of thermal decomposition to PbI_2.[15,23] We also note a flame-like pattern progressing from left to right across photonic annealed films with increasing exposure. This is a result of the forced directional airflow across the sample intended to protect the flash bulb from evolved solvents during annealing. This airflow blows CH_3NH_3Cl evolved from the precursor during annealing across the sample surface, causing the light to be occluded behind the so-called "forced-air front". This light attenuation results in regions below the evolved CH_3NH_3Cl being annealed to a lesser degree than more exposed areas. A schematic diagram further illustrating this phenomena is shown in Figure S1 in the ESI†.

The option of drying the deposited precursor prior to flash annealing would likely improve film reproducibility. The effects of solvent evaporation causing discontinuous annealing would be greatly reduced in this case. In addition, using perovskite precursor solutions eschewing $PbCl_2$, such as those containing only CH_3NH_3I and PbI_2, may improve film reproducibility as no CH_3NH_3Cl would be evolved, occluding the film during crystallisation.

As well as colour differences across the surface of photonic annealed samples, there also appeared to be variations in surface roughness within the same film. In some regions, the perovskite films appear extremely smooth and reflective whereas other regions show a more "hazy" surface. Surface roughness measurements were performed using a profilometer and found typical Ra values of 5 nm and 100 nm for respective smooth and reflective regions, with the 230 nm thick bare Al_2O_3 scaffold measuring at 3 nm Ra. Corresponding surface profile plots are seen in Figure S2 in the ESI†. Figure 2 shows SEM micrographs of different regions of a photonic annealed film, as well as cross-section schematics suggesting the distribution of perovskite mate-rial throughout the film: Section "a" represents a characteristic hazy region, whereas "b" represents a typical smooth and reflective region. The micrographs demonstrate that, in the case of the smooth sections, the entire bulk of perovskite material is confined within the mesoporous Al_2O_3 film. In the more hazy section, outcrops of perovskite material are seen above the Al_2O_3 film in a structure more similar to that observed in devices which have a perovskite capping layer that extends beyond that of the mesoporous structure.[24] We suggest that the lack of a discrete and continuous capping layer across the film's surface is due to the near-instantaneous phase transformation undergone during annealing which may have lead to precursor being ejected from the glass surface.

Photoluminescence intensity measurements for the photonic and hotplate annealed films are shown in Figure 3a. There is a blue-shift in emission from hotplate to photonic annealing which is attributed to the smaller crystal sizes obtained when using such a rapid heating method. XRD measurements for hotplate and photonic annealed films, seen in Figure 3b confirm these hypotheses.

While the films shown in Figure 1 exhibit yellowed regions indicating the presence of PbI_2, the XRD and photoluminescence measurements shown in Figure 3 were performed on samples further optimised between 1.0 ms and 1.2 ms which showed no visual evidence of PbI_2. The spectra for photonic annealed perovskite films shows reduced preferential orientation compared to hotplate annealed counterparts as a result of this scaffold confinement. In slow hotplate annealing, grains have more time to grow into large, oriented crystals as seen in Figure 2. By comparison, photonic annealed films are crystallised in timeframes 4.5 million times faster using entirely different crystallisation kinetics, thus leading to smaller grain sizes.

An analysis of J-V statistics is presented in Figure 4. While overall PCEs in photonic annealed cells are lower than hotplate annealed devices the V_{OC} remains high in the optimised group. This would indicate that the drop in performance is not due to pinhole formation or poor perovskite film coverage as this has been found to reduce voltages in perovskite devices due to recombination at the interface between the c-TiO_2 and Spiro-OMeTAD that arises inside pinholes.[25] The high V_{OC} indicates good coverage and in-

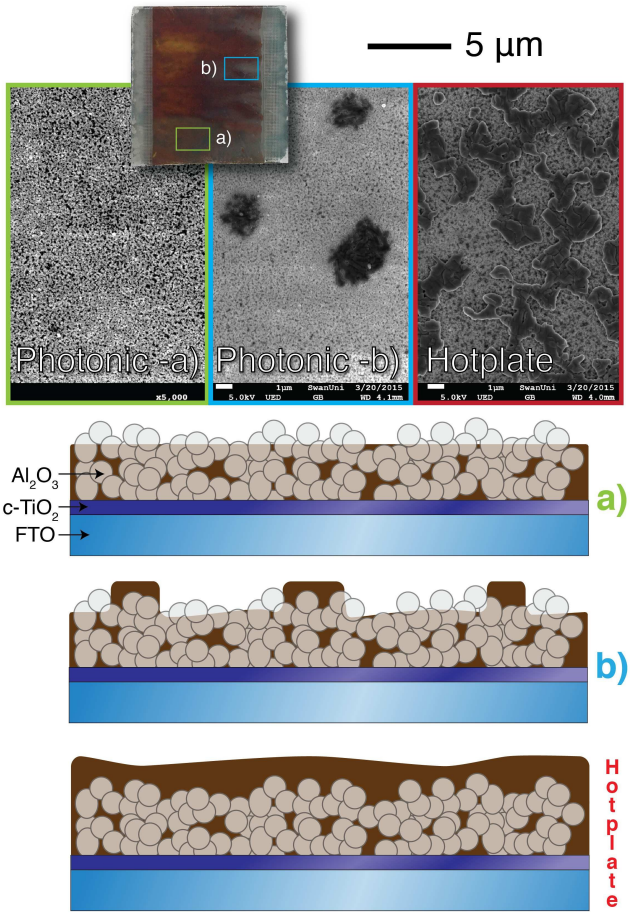

Fig. 2 Top: SEM micrographs showing different surface regions of a photonic annealed perovskite film. a) Represents a reflective region whereby the perovskite material appears to be confined within the mesoporous scaffold. b) Represents a "hazy" region where perovskite "islands" protrude through the scaffold surface. Also included is a micrograph of a hotplate-annealed perovskite film which shows a more continuous perovskite capping layer. Bottom: Schematic cross-section representations of the corresponding films, whereby a) indicates total perovskite confinement within the scaffold, b) shows some capping layer outcrops above the Al_2O_3, and c) shows a near continuous perovskite capping layer.

timate contact between the electron selective TiO_2 compact layer and perovskite film. This suggests that, while annealing is driven by direct exposure of the perovskite precursor to light instead of a traditional substrate-driven thermal reaction, there is sufficient photon penetration to anneal perovskite at the c-TiO_2 interface. Short-circuit current density and fill factor are markedly lower in the fast processed devices. The drop in J_{SC} is attributed to the lack of perovskite capping layer above the Al_2O_3 scaffold, which limits the thickness. The lower fill factors arise in part due to an apparent increase in series resistance, which can be attributed to poor contact between the Spiro-OMeTAD and the perovskite layer. The lack of capping layer in the photonically annealed devices means that instead of forming a conformal heterojunction (as would be expected in the presence of a capping layer), the Spiro-OMeTAD makes contact with outcrops of Al_2O_3, as well as the perovskite, reducing the effective contact area and thereby

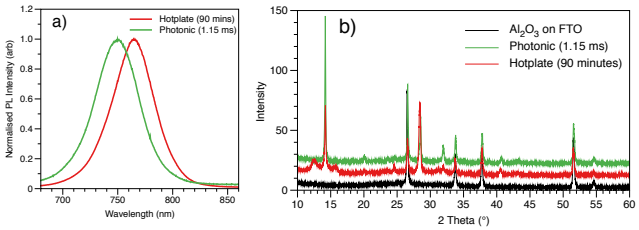

Fig. 3 a) Photoluminescent intensity for hotplate and photonic annealed perovskite films. b) X-ray diffraction spectra for mp-Al_2O_3 coated FTO, photonic annealed and hotplate annealed films.

introducing series resistance losses. Despite remarkably low annealing times, a clear optimum flash length may be ob-served in Figure 4. between 1,125 μs and 1,175 μs pulse exposure which may at first seem problematic as the processing window seems rather limited, but looking closer at the statistical JV data it can be seen that there are significant improvements in performance at an exposure time of 1150 μs compared to exposure times of just $\pm 50\,\mu s$. This indicates the degree of precision and accuracy of the instruments control system that would be essential to make this a commercially viable technique for perovskite solar cell manufacture.

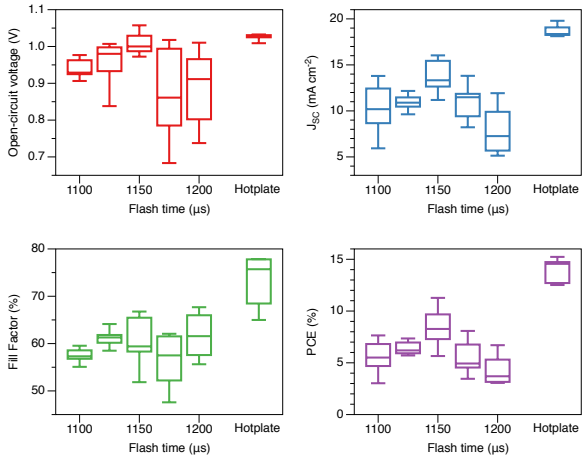

Fig. 4 Statistical analysis of J-V parameters for photonic annealed cells processed at different exposure times, as well as hotplate annealed counterparts.

Transient Photovoltage (TPV) and Transient Photocurrent (TPC) decay experiments were carried out on a selection of devices. Data from these experiments are presented in Figure 5. Figure 5a shows the TPV lifetime of a hotplate annealed device and that of a photonically annealed device. The TPV decay curves in this case were multi-exponential as observed elsewhere.[25] In line with the reasoning of O'Regan and coworkers,[26] to extrapolate the decay lifetimes we fit a double exponential function to the decay and take the faster of the two time constants as the effective recombination lifetime. Looking at Figure 5a one can see why V_{OC} remains high in photonically annealed devices. It appears that recombination is slower (for a given V_{OC}) in the photonically annealed device. This is further evidence of a good conformal contact between c-TiO_2 and perovskite layer. For an

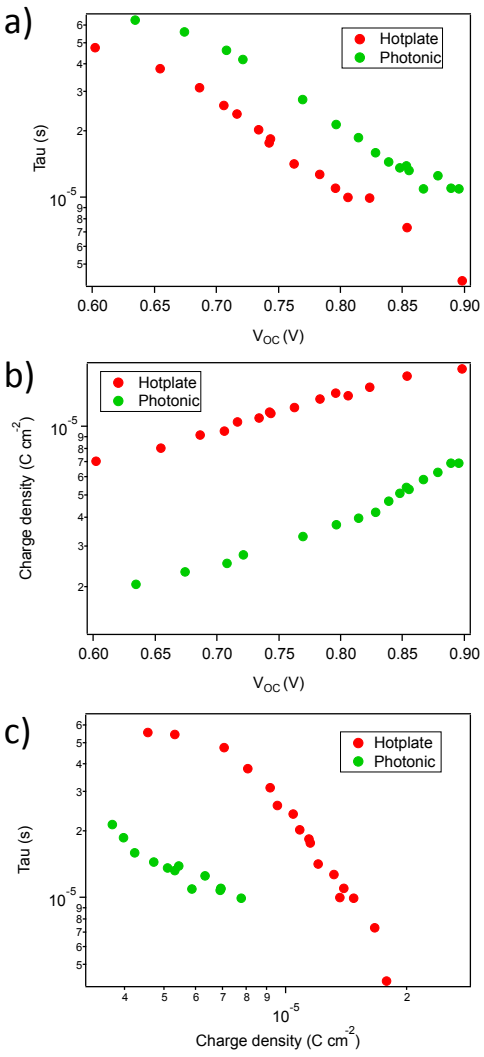

Fig. 5 Comparisons between hotplate and photonically annealed perovskite solar cells: a) Recombination lifetimes of devices for a given V_{OC}. b) Charge density for a given V_{OC}. c) Recombination lifetime for a given charge density.

explanation of the drop in J_{SC}, the charge density of the devices can be obtained from their respective TPV and TPC data via calculation of the differential capacitance.[26] This data is shown in Figure 5b and it is clear that the charge density (C cm^{-2}) in photonically annealed devices is significantly lower, supporting the hypothesis that the poorer performance is due to a thinner perovskite film thickness or lack of a capping layer. Having identified the effective recombination lifetime and charge density, we can look at recombination lifetime for a given charge density (C cm^{-2}), this is shown in Figure 5c. Conversely to Figure 5a, Figure 5c shows that recombination (for a given charge density) is faster in the photonically annealed device. This primarily results from the thinner perovskite layer and so emphasises the need for further optimisation of the technique or process conditions so that perovskite film thickness and capping layers remain favourable for increased device performance.

Despite the aforementioned drop in photonically annealed device current and fill factor compared to hotplate processed cells, a maximum PCE of 11.3% is produced compared to 15.2% for the conventionally produced cell as seen in Table 1. Figure 6a shows J-V curves for the best performing photonic and hotplate processed devices, whereas Figure 6b shows time-dependent lamp power density measurement extracted from the photonic sintering tool corresponding to a pulse profile yielding the highest performing cell.

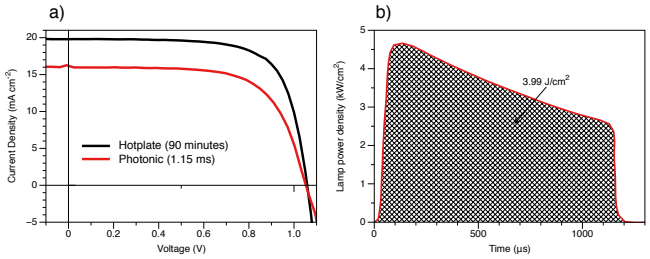

Fig. 6 a) J-V curves for highest performing photonic and hotplate annealed perovskite solar cells. b) A time-dependent power density plot of the flash used to anneal the highest performing device.

The decay of lamp power over time is a result of the instruments capacitors draining as the flash bulb is engaged as shown in Figure 6b. It was found that "square" energy profiles could only be achieved using short exposure times and lower voltages than those required to fully anneal perovskite films in a single flash. Such uniform profiles would reduce the complexity of obtaining optimal flash annealing parameters. Interestingly, the energy density required to anneal the highest performing perovskite film, 3.99 J cm^{-2}, corresponds to between 10-130 times the minimal erythemal dose required to sunburn skin depending on skin color.[27] Despite these seemingly high energies, the process is remarkably more efficient than hotplate annealing which was measured using an electricity usage monitor to be ca. 200 J cm^{-2} in order to maintain a laboratory hotplate at 100 °C for 90 minutes. This figure rises significantly if the hotplate's initial heating is included. This 50 times reduction in power requirement poses a substantial cost saving in the case of commercial production compared to hotplate annealing.

Table 1 Hero cell efficiency data for both conventional and photonic annealed perovskite solar cells.

Annealing method	V_{OC} (V)	J_{SC} (mA cm^{-2})	Fill Factor (%)	PCE (%)
Hotplate	1.03	19.8	75	15.23
Photonic	1.05	16.0	67	11.27

3 Conclusions

In conclusion, we have demonstrated that the time and energy required to fully anneal $CH_3NH_3PbI_{3-x}Cl_x$ perovskite films may be drastically reduced using a novel flash annealing process. In as little as 1.15 ms, a spin-coated precursor solution may be fully annealed using an intense flash of white light and yield PCEs in excess of 11% compared to 15% in a 90 minute, inert atmo-

sphere, hotplate annealed cell. Such a rapid annealing process introduces new crystallisation kinetics which yield notably smaller perovskite crystals compared to conventionally processed films, as proven using PL and XRD measurements. While overall PCEs in fast-processed devices falls short of the conventional processing method, the amount of energy and time required to achieve such films is dramatically reduced. This work presents some initial optimisation of the photonic annealing process however with additional control of the photonic pulsing which inhibits the removal of the capping layer, devices with performance equivalent to conventionally produced devices are possible. In summary this process represents a 4.5 million times reduction in processing time and a 50 times reduction in the power requirements, both critical contributors towards the successful commercial production of perovskite photovoltaics.

4 Experimental

4.1 Device fabrication

Working electrodes were prepared by depositing a compact TiO_2 (c-TiO_2) layer upon a 3 mm thick FTO glass substrate (7Ω sq^{-1}, Ra: 12 nm, NSG Pilkington) through spray pyrolysis at 450 °C A mesoporous Al_2O_3 (mp-Al_2O_3) film was next deposited by diluting a dispersion of Al_2O_3 nanoparticles (Sigma-Aldrich PN:702129) in isopropanol (1:2 by volume), and spin coating for 60 s at 4,500 rpm. Upon drying at 150 °C for 10 minutes on a hotplate, a 230 nm scaffold was produced. A mixed-halide perovskite precursor was prepared in DMF by dissolving a 40wt%, 3:1 molar ratio of CH_3NH_3I and $PbCl_2$ before spin coating onto the mp-Al_2O_3 layer for 45 seconds at 2,000 rpm. In the case of photonic annealing, this process was performed in air (20 °C, c.50% RH), whereas hotplate-annealed reference devices were deposited and annealed in a N_2-filled glovebox (<0.5 ppm H_2O, <0.5 ppm O_2, MBraun). Hotplate annealed samples underwent 100 °C for 90 minutes, followed by 120 °C for 10 minutes as described elsewhere.[12] The typical term "photonic curing" was used to describe subjection of a precursor-coated sample to xenon flash-bulb emission over very small time scales. Photonic cured samples were immediately transferred from spin-coater to photonic curing tool (PulseForge 1300, Novacentrix) and flash annealed in milliseconds without prior or subsequent heating. Distance between lamp and sample was fixed at a point recommended by the manufacturer, initial trials undertaken at points outside the recommended distance showed much greater variability due to irradiance irregularity and so are not shown here. Lamp voltage was maintained at 500 V. Upon completion of the annealing step, samples were cooled to room temperature before a solution containing 2-7,7-tetrakis(N,N-di-p-methoxyphenylamine)-9,9 17-spirobifluorene (spiro-OMeTAD) in chlorobenzene and additives (10 μl/ml tBP, 32 μl/ml Li-TFSI solution: 600 mM in acetonitrile) was spin-coated onto the perovskite film before 80 nm thick Au contacts were evaporated at 10^{-4} torr.

4.2 Characterisation

Scanning electron microscopy imaging of photonic and hotplate annealed samples were collected using a JSM-7800F field emission gun electron microscope from Jeol (USA), with a 5 kV beam, 10 μA at approximately 4.1 mm working distance. X-ray diffraction analyses of the crystalline properties of the annealed films were carried out using a D8 Discover instrument from Bruker (Germany) with a CuKα beam at 40 kV and 40 mA and scan parameters of 0.1 s/step at 0.01 2θ step size.

Transient photovoltage and photocurrent decays were measured as described previously.[28] The white bias light was provided by a BRIDGELUX 9000 lumen LED array (Farnell) whilst the pulse light was provided by a OSLON PowerCluster green LED array (RS). Pulse intensity was chosen to ensure ΔV remained within the small perturbation regime. A pulse length of 10 μs was utilised and was generated via a fast MOSFET transistor controlled by a National Instruments USB-6251 data acquisition board (DAQ) and WaveMetrics IGOR Pro software. Voltages were measured directly using the DAQ. Currents were measured by the DAQ as a voltage drop across a 30 Ω resistor. The open-circuit voltage was allowed to equilibrate for >60 s before the perturbation pulse was fired. The variance in photovoltage in the preceding 10 s before the perturbation pulse was fired was found to be, on average, <1.2 mV. A biphasic photovoltage decay was observed and fit with a double exponential function. The faster of the two resultant time constants was taken as the effective recombination lifetime. Differential capacitance and charge density were calculated as described elsewhere.[26]

Emission spectra of perovskite thin films were observed using a Olympus BX51 M microscope coupled with an Ocean Optics USB2000+ spectrometer and optical fiber. The optical fiber was placed down the eyepiece of the microscope to collect the emission spectrum of the whole imaged area. Samples were illuminated with a UV-mercury lamp (100 W Ushio Olympus) through a filter block consisting of an excitation filter (TXRED filter CWL = 559 nm) a dichroic mirror (TXRED reflection band = 533-580 nm, transmission band = 595-800 nm) and an emission filter (665 nm Longpass). Emission spectra were measured in-situ simultaneously to image collection through averaging 50 scans with an integration time of 0.1 s. All observations were carried out at 22 °C.

Masked devices (0.09 cm^2) were tested under a class AAA solar simulator (Newport Oriel Sol3A) at AM1.5 and 100 mW cm^{-2} illumination conditions calibrated against a KG5 filtered silicon reference cell (Newport Oriel 91150-KG5) using a Keithley 2400 source meter. Current-voltage sweeps were performed from forward-to-reverse bias at a rate of 0.1 V s^{-1}.

5 Acknowledgements

The authors recognise the financial support of the EPSRC and Innovate UK for the SPECIFIC Innovation and Knowledge Centre (grant numbers EP/I019278/1, EP/K000292/1, EP/L010372/1) the SuperSolar flexible funding (EP/5017361/1) and the Welsh Government for support to the Sêr Solar program. We would like to acknowledge funding by the European Social Fund (ESF) through the European Union's Convergence program administered by the Welsh Government as well as Tata Steel Europe for additional student funding. We would especially like to thank Novacentrix for use of their PulseForge 1300 tool. M.J.C. would like to thank Piers Barnes, Brian O'Regan, James Durrant, Scott

Wheeler and Daniel Bryant of Imperial College London for advice and discussions on TPV measurements.

References

1 A. Kojima, K. Teshima, Y. Shirai and T. Miyasaka, *Journal of the American Chemical Society*, 2009, **131**, 6050–6051.

2 H.-S. Kim, C.-R. Lee, J.-H. Im, K.-B. Lee, T. Moehl, A. Marchioro, S.-J. Moon, R. Humphry-Baker, J.-H. Yum, J. E. Moser, M. Gratzel and N.-G. Park, *Scientific Reports*, 2012.

3 J. M. Ball, M. M. Lee, A. Hey and H. J. Snaith, *Energy and Environmental Science*, 2013, **6**, 1739–1743.

4 J. H. Heo, S. H. Im, J. H. Noh, T. N. Mandal, C.-S. Lim, J. A. Chang, Y. H. Lee, H.-j. Kim, A. Sarkar, N. K., M. Gratzel and S. I. Seok, *Nature Photonics*, 2013, **7**, 486–491.

5 M. J. Carnie, C. Charbonneau, M. L. Davies, J. Troughton, T. M. Watson, K. Wojciechowski, H. Snaith and D. A. Worsley, *Chemical Communications*, 2013, **49**, 7893–7895.

6 J. Burschka, N. Pellet, S.-J. Moon, R. Humphry-Baker, P. Gao, M. K. Nazeeruddin and M. Gratzel, *Nature*, 2013, **499**, 316–319.

7 Y. Wu, A. Islam, X. Yang, C. Qin, J. Liu, K. Zhang, W. Peng and L. Han, *Energy and Environmental Science*, 2014, **7**, 2934–2938.

8 L. Hu, J. Peng, W. Wang, Z. Xia, J. Yuan, J. Lu, X. Huang, W. Ma, H. Song, W. Chen, Y.-B. Cheng and J. Tang, *ACS Photonics*, 2014, **1**, 547–553.

9 M. Liu, M. Johnston and H. Snaith, *Nature*, 2013, **501**, 395–398.

10 Q. Chen, H. Zhou, Z. Hong, S. Luo, H.-S. Duan, H.-H. Wang, Y. Liu, G. Li and Y. Yang, *Journal of the American Chemical Society*, 2014, **136**, 622–625.

11 N. J. Jeon, J. H. Noh, Y. C. Kim, W. S. Yang, S. Ryu and S. I. Seok, *Nature Materials*, 2014, **13**, 897–903.

12 M. Saliba, K. W. Tan, H. Sai, D. T. Moore, T. Scott, W. Zhang, L. A. Estroff, U. Wiesner and H. J. Snaith, *The Journal of Physical Chemistry C*, 2014, **118**, 17171–17177.

13 A. T. Barrows, A. J. Pearson, C. K. Kwak, A. D. F. Dunbar, A. R. Buckley and D. G. Lidzey, *Energy and Environmental Science*, 2014, **7**, 2944–2950.

14 C. Bi, Y. Shao, Y. Yuan, Z. Xiao, C. Wang, Y. Gao and J. Huang, *Journal of Materials Chemistry A*, 2014, **2**, 18508–18514.

15 A. Dualeh, N. Tétreault, T. Moehl, P. Gao, M. K. Nazeeruddin and M. Grätzel, *Advanced Functional Materials*, 2014, **24**, 3250–3258.

16 A. E. Williams, P. J. Holliman, M. J. Carnie, M. L. Davies, D. A. Worsley and T. M. Watson, *Journal of Materials Chemistry A*, 2014, **2**, 19338–19346.

17 J. Troughton, C. Charbonneau, M. J. Carnie, M. L. Davies, D. A. Worsley and T. M. Watson, *Journal of Materials Chemistry A*, 2015, 9123–9127.

18 K. Schroder, S. McCool and W. Furlan, *Presented at NSTI Nanotech May*, 2006, **7**, 11.

19 M. Hosel and F. C. Krebs, *Journal of Materials Chemistry*, 2012, **22**, 15683–15688.

20 R. Søndergaard, M. Hösel, D. Angmo, T. T. Larsen-Olsen and F. C. Krebs, *Materials Today*, 2012, **15**, 36–49.

21 F. Di Giacomo, V. Zardetto, A. D'Epifanio, S. Pescetelli, F. Matteocci, S. Razza, A. Di Carlo, S. Licoccia, W. M. M. Kessels, M. Creatore and T. M. Brown, *Advanced Energy Materials*, 2015, **5**, 1614–6840.

22 C. J. Stolle, T. B. Harvey, D. R. Pernik, J. I. Hibbert, J. Du, D. J. Rhee, V. A. Akhavan, R. D. Schaller and B. A. Korgel, *The Journal of Physical Chemistry Letters*, 2014, **5**, 304–309.

23 T. Supasai, N. Rujisamphan, K. Ullrich, A. Chemseddine and T. Dittrich, *Applied Physics Letters*, 2013, **103**, 183906.

24 G. E. Eperon, V. M. Burlakov, A. Goriely and H. J. Snaith, *ACS Nano*, 2014, **8**, 591–598.

25 M. J. Carnie, C. Charbonneau, M. L. Davies, B. O. Regan, D. A. Worsley and T. M. Watson, *Journal of Materials Chemistry A*, 2014, **2**, 17077–17084.

26 B. C. O'Regan, P. R. F. Barnes, X. Li, C. Law, E. Palomares and J. M. Marin-Beloqui, *Journal of the American Chemical Society*, 2015, **137**, 5087–5099.

27 W. Westerhof, O. Estevez-Uscanga, J. Meens, A. Kammeyer, M. Durocq and I. Cario, *Journal of Investigative Dermatology*, 1990, **94**, 812–816.

28 P. R. F. Barnes, K. Miettunen, X. Li, A. Y. Anderson, T. Bessho, M. Gratzel and B. C. O'Regan, *Advanced Materials*, 2013, **25**, 1881–1922.